

Coherent imaging of extended objects

E. Brainis ^{*}, C. Muldoon, L. Brandt, A. Kuhn

Department of Physics, University of Oxford, Parks Road OX1 3PU Oxford, United Kingdom

Abstract

When used with coherent light, optical imaging systems, even diffraction-limited, are inherently unable to reproduce both the amplitude and the phase of a two-dimensional field distribution because their impulse response function varies slowly from point to point (a property known as non-isoplanatism). For sufficiently small objects, this usually results in a phase distortion and has no impact on the measured intensity. Here, we show that the intensity distribution can also be dramatically distorted when objects of large extension or of special shapes are imaged. We illustrate the problem using two simple examples: the pinhole camera and the aberration-free thin lens. The effects predicted by our theoretical analysis are also confirmed by experimental observations.

Key words: Coherent Optics, Diffraction, Imaging, Optical Instruments, Lithography, Microscopy, Holography

PACS: 42.30.Kq, 42.30.Va, 42.30.Lr

1. Introduction

Current technology, especially the ability to manufacture aspherical surfaces, allows lenses and mirrors to be designed that minimize the most important geometrical aberrations. Such optical elements are nearly ideal instruments obeying the laws of Gaussian optics even for far off-axis points and non-paraxial rays. Self-luminous objects or objects illuminated with *incoherent* light can be imaged with high fidelity. The quality of the resulting image is merely fixed by the resolution of the instrument which is related to its numerical aperture. The instrument itself is said to be *diffraction-limited* and can be considered as a linear filter for the intensity of light [1,2].

When imaging objects with *coherent* light, the conditions for accurate image formation are more severe since both the relative amplitudes and the relative phases of the object points have to be mapped to the corresponding image points (up to the resolution capability of the instrument). This only happens if the response of the optical instrument to the field from a given point source is independent of its position in the object plane, or in other words, if the coherent impulse response [1,2] of the system is *space-independent*. The instrument then acts as a *linear filter* for the complex field amplitude. According to the terminology of [1], such an instrument is said to be *isoplanatic*. In gen-

eral, even aberration-free optical instruments designed to map some planar object to an image plane under incoherent illumination do not meet this condition. Some spatial phase distortion is unavoidably introduced, which, when combined with a finite resolution, severely modifies the intensity distribution of the image. This was first recognized by Dumontet [3], and later by Tichenor and Goodman [4], who showed that a thin lens can only be considered as an isoplanatic system if both the object and the image lie on spherical surfaces \mathcal{S}_o and \mathcal{S}_i , tangent to the geometrical-optics object and image planes \mathcal{O} and \mathcal{I} respectively, and having their center of curvature in the plane of the lens (see Sec. 3).

In practice, an aberration-free optical instrument can be treated as an ideal coherent-light imaging system whenever the spherical surfaces \mathcal{S}_o and \mathcal{S}_i can be approximated by their tangent planes \mathcal{O} and \mathcal{I} . We emphasize that this is only viable when the object to be imaged is very small and lies close to the optical axis. A weaker imaging condition has been obtained by Tichenor and Goodman who showed that non-isoplanatism of a thin lens has a negligible effect on the *intensity distribution* of the image if the object diameter is smaller than about a quarter of the lens diameter [4]. In this paper, we investigate the effect of non-isoplanatism on coherent image formation when this condition is not met. That situation may be encountered in many fields of optics where large-sized objects are imaged through powerful limited-aperture instruments, as in coherent far-field microscopy, optical lithography [5], holographic data-storage

^{*} Corresponding author.

Email address: e.brainis1@physics.ox.ac.uk (E. Brainis).

[6], and dipole-trapping of neutral atoms [7]. In particular arrays of coherently emitting point sources, like individual trapped atoms excited by the same laser beam [8,9], will be subject to the phenomena discussed here. Effects similar to those that we described in the context of imaging are also expected when lenses are used to perform the spatial Fourier transform of a two-dimensional field distribution, as or holographic dipole-trapping of atoms [10].

2. Non-isoplanatism of a pinhole camera

The problem of non-isoplanatism can be best understood by considering the simple example of coherent image formation through a pinhole camera (Fig. 1).

Consider the following situation: Two mutually coherent point-objects, P_1 and P_2 , are imaged through a small pinhole (of radius a) from an object plane \mathcal{O} to an image plane \mathcal{I} . We call $(x_{o,k}, y_{o,k})$ the transverse coordinates of the point sources P_k ($k \in \{1, 2\}$), and $(x_{i,k}, y_{i,k})$ the transverse coordinates of their geometrical images P'_k . For simplicity, we chose $y_{o,k} = y_{i,k} = 0$ and assume that the point sources emit in phase. We assume that the pinhole is so small that the resolution is limited by diffraction. The “images” of P_1 and P_2 are two Airy patterns centered on the geometrical image points P'_1 and P'_2 . Let’s consider that P'_1 and P'_2 are at the resolution limit according to the Rayleigh criterion $x_{i,1} - x_{i,2} = 0.61\lambda z_i/a$. Due to the geometry displayed in Fig. 1, the relative phase of their respective Airy patterns is $\phi = 2\pi(r_1 - r_2)/\lambda$. This shows that *the phase relation between points is not mapped properly from the object plane to the image plane*. Furthermore, *the relative phase ϕ varies as a function of $x_{o,m} \equiv (x_{o,1} + x_{o,2})/2$, the mean distance of the point sources to the optical axis*. The phase ϕ is obviously null if $x_m = 0$, but it already reaches the value $\pi/2$ when $|x_{o,m}| = a/2.44$. Since a is usually about 1 mm for a pinhole camera, ϕ varies extremely rapidly when the two point sources are moved over the object plane. Fig. 2 shows the intensity distribution in the image plane resulting from the interference of two Airy patterns with relative phase

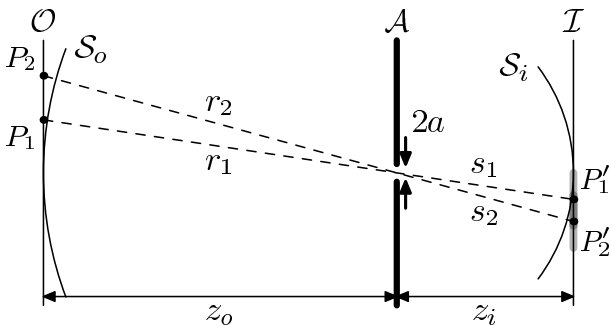


Fig. 1. Scheme for coherent image formation by a pinhole camera. The points P'_1 and P'_2 in the image plane \mathcal{I} are the geometrical images of the point objects P_1 and P_2 in the object plane \mathcal{O} . The light-gray zones around P'_1 and P'_2 in the \mathcal{I} -plane represent the individual diffraction patterns resulting from illumination of the pinhole by P_1 and P_2 respectively. The dark-gray zone represents the area where the individual diffraction patterns overlap and interfere.

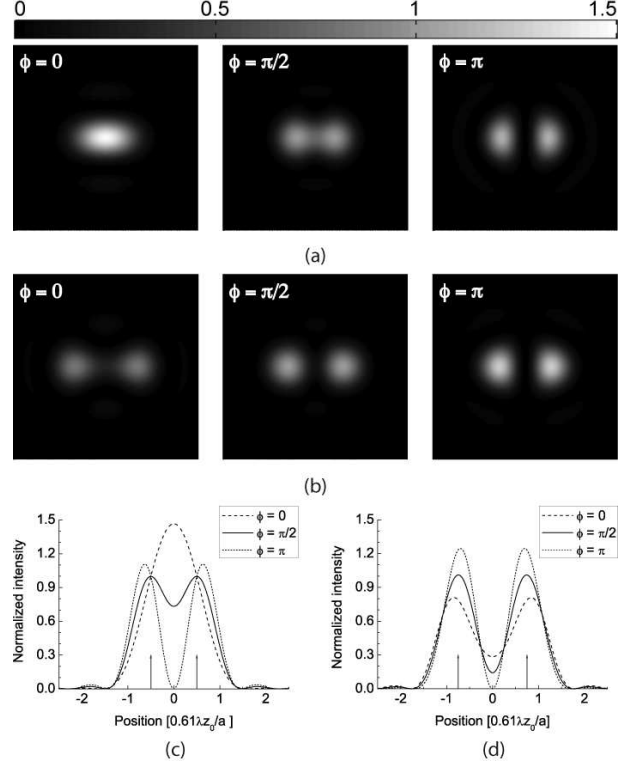


Fig. 2. Intensity profile in the image plane of a diffraction-limited pinhole camera due to the interference of the Airy patterns of two coherent point sources. The distance $|x_{o,1} - x_{o,2}|$ between the sources is equal to (a) $0.61\lambda z_o/a$ (the Rayleigh resolution limit), and (b) $0.915\lambda z_o/a$ (1.5 times the Rayleigh resolution limit). The Airy patterns have been normalized so that their peak intensity is 1. Panel (c) and (d) show the intensity profiles along the x -axis corresponding to the images in panel (a) and (b), respectively. Vertical arrows in panels (c) and (d) point the positions of the centers of the interfering Airy patterns.

$\phi = 0, \pi/2$, and π . In panel (a) the distance between the sources corresponds to the Rayleigh resolution criterion, as discussed before; in panel (b) this distance is increased by a factor of 1.5. Panel (c) and (d) display the intensity profile along the x -axis for images in panel (a) and (b), respectively. Note that the intensity distribution for $\phi = \pi/2$ is the same as for incoherent sources. Because of this interference, the image points may be unresolved even if their relative positions fulfill the Rayleigh criterion.

The preceding example shows that different intensity distributions must be expected from identical object patterns depending on their positions in the object plane. This is due to an incorrect phase mapping between the object and image plane. The relative phase of an object point and its image depends on the position of the point source in the object plane. We refer to this situation as the *non-isoplanatism* of coherent imaging. Considering the pinhole camera as a linear optical system [2], non-isoplanatism is related to the space-variance of its impulse response. We develop this point of view hereafter.

Since the pinhole camera is a linear system, the complex field amplitudes in the object and image planes, $U_o(x_o, y_o)$ and $U_i(x_i, y_i)$ satisfy the integral relation

$$U_i(x_i, y_i) = \iint h(x_i, y_i | x_o, y_o) U_o(x_o, y_o) dx_o dy_o.$$

The impulse response of the camera (in the paraxial and far-field approximation) is given by the Fraunhofer integral

$$\begin{aligned} h(x_i, y_i | x_o, y_o) &= \frac{1}{\lambda^2} \frac{e^{i2\pi(r+s)/\lambda}}{rs} \iint_{\mathcal{A}} e^{-i2\pi(f_x \xi + f_y \eta)} d\xi d\eta, \\ &= \frac{1}{\lambda^2} \frac{e^{i2\pi(r+s)/\lambda}}{rs} \delta_a(f_x, f_y), \end{aligned} \quad (1)$$

where (x_o, y_o) are the coordinates of the point source in the object plane, (x_i, y_i) are the coordinates of the ‘‘observation point’’ in the image plane. The integration domain \mathcal{A} is the pinhole opening disc, while

$$\begin{aligned} r &= \sqrt{x_o^2 + y_o^2 + z_o^2}, \\ s &= \sqrt{x_i^2 + y_i^2 + z_i^2} \end{aligned}$$

are the distances from the point source and the observation point to the pinhole center, and

$$\begin{aligned} f_x &= \frac{1}{\lambda} \left(\frac{x_i}{s} + \frac{x_o}{r} \right), \\ f_y &= \frac{1}{\lambda} \left(\frac{y_i}{s} + \frac{y_o}{r} \right) \end{aligned}$$

are the spatial frequencies of the plane waves diffracted by the pinhole. On the second line of (1), the function

$$\delta_N(x, y) = |N| \frac{J_1(2\pi N \sqrt{x^2 + y^2})}{\sqrt{x^2 + y^2}} \quad (N \in \mathbb{R}_0) \quad (2)$$

has been introduced ($J_1(x)$ is a Bessel function of first kind). Its square $\delta_N^2(x, y)$ is the usual intensity point spread function or Airy pattern of diffraction-limited optical systems and it is normalized so that $\lim_{|N| \rightarrow \infty} \delta_N(x, y) = \delta(x, y)$ (the Dirac distribution). The ‘‘scaling’’ property, $\delta_N(Cx, Cy) = \delta_{CN}(x, y)/C^2$ for any $C \in \mathbb{R}_0$, can be used to simplify (1):

$$\begin{aligned} h(x_i, y_i | x_o, y_o) &= |M| e^{i\frac{2\pi}{\lambda}(r+s)} \times \\ &\delta_{\frac{a}{\lambda s}}(x_i - Mx_o, y_i - My_o), \end{aligned} \quad (3)$$

where $M = -s/r$ is the geometric *magnification ratio* of the camera. Note that we can make the approximation $M \approx -z_i/z_o$ because r and s vary only very slightly over the object and image planes. For the same reason, $\delta_{a/(\lambda s)}(x, y) \approx \delta_{a/(\lambda z_i)}(x, y)$.

The phase factor in Eq. (3) plays an important role. If the phase factor were not there, the impulse function corresponding to any point (x_o, y_o) lying in the object plane would be the same as the impulse function of the origin $(0, 0)$, but translated to the geometrical image point (Mx_o, My_o) ; in that case, the system would be space-invariant, or *isoplanatic*, and the image of a coherent object with field amplitude $U_o(x_o, y_o)$ could be computed by simply convoluting $U_o(x_o, y_o)$ with the impulse function. In other words, the pinhole camera would act as a linear

filter that reproduces the object $U_o(x_o, y_o)$ with a lower resolution. The example of Fig. 2 clearly shows that this is not the case. Because of the phase factor, the impulse response function is different for different points in the object plane. This creates interference patterns that modify the image more significantly than a simple blur. The image of a field profile $U_o(x_o, y_o)$ is given by

$$\begin{aligned} U_i(x_i, y_i) &= \frac{1}{|M|} e^{i\frac{2\pi}{\lambda}s} \iint U_o(x_o, y_o) e^{i\frac{2\pi}{\lambda}r} \\ &\delta_{\frac{a}{\lambda z_o}} \left(\frac{x_i}{M} - x_o, \frac{y_i}{M} - y_o \right) dx_o dy_o. \end{aligned} \quad (4)$$

To establish Eq. (4), we make use of the fact that

$$\delta_{\frac{a}{\lambda z_i}}(x_i - Mx_o, y_i - My_o) = \frac{1}{M^2} \delta_{\frac{a}{\lambda z_o}} \left(\frac{x_i}{M} - x_o, \frac{y_i}{M} - y_o \right)$$

can be considered either as a function of (x_i, y_i) , the usual Airy pattern centered on the geometrical image point (Mx_o, My_o) , or as a function of (x_o, y_o) centered on the object point $(x_i/M, y_i/M)$. Note that in the first interpretation, the first-zero full-width of the Airy pattern $e_i = 1.22\lambda z_i/a$ represents the region of the image plane most influenced by the field originating from the point source at (x_o, y_o) in the object plane. In the second interpretation, the first-zero full-width of the Airy pattern $e_o = 1.22\lambda z_o/a$ represents the area of the object plane that most contributes to the field at the observation point (x_i, y_i) in the image plane. In the *non-isoplanatic* situation described by Eq. (4), important interferences occur when the phase factor $\exp[i\frac{2\pi}{\lambda}r]$ cannot be considered as constant over the circular region of area $\pi(e_o/2)^2$ centered on $(x_i/M, y_i/M)$ in the object plane.

It is interesting to note that isoplanatism is recovered when one considers the imaging problem from \mathcal{S}_o to \mathcal{S}_i (see Fig. 1), where \mathcal{S}_o (\mathcal{S}_i) is a spherical surface of radius z_o (z_i) centered on the pinhole, and having its vertex on \mathcal{O} (\mathcal{I}). The spherical field distributions on \mathcal{S}_o and \mathcal{S}_i are described by the amplitudes $U_{\mathcal{S}_o}(x_o, y_o)$ and $U_{\mathcal{S}_i}(x_i, y_i)$, respectively (z -coordinates are dependent variables). These are related to the field amplitudes on \mathcal{O} and \mathcal{I} by a phase relation: $U_{\mathcal{S}_o}(x_o, y_o) = U_o(x_o, y_o) \exp[i2\pi(r - z_o)/\lambda]$ and $U_{\mathcal{S}_i}(x_i, y_i) = U_i(x_i, y_i) \exp[-i2\pi(s - z_i)/\lambda]$. Inserting these relations into Eq. (4) and removing the constant phase factor $\exp[i2\pi(z_o + z_i)/\lambda]$ one gets:

$$\begin{aligned} U_{\mathcal{S}_i}(x_i, y_i) &= \frac{1}{|M|} \iint U_{\mathcal{S}_o}(x_o, y_o) \\ &\delta_{\frac{a}{\lambda z_o}} \left(\frac{x_i}{M} - x_o, \frac{y_i}{M} - y_o \right) dx_o dy_o \end{aligned} \quad (5)$$

which is a convolution relation, as expected for an isoplanatic imaging system. The physical reason why isoplanatism is recovered when the object lies on the spherical surface \mathcal{S}_o is simple to understand: since all the point sources are at same distance z_o from the pinhole, their point spread functions always interfere constructively. Note that there is no real need to measure the image on \mathcal{S}_i for it only

differs from the image in the plane \mathcal{I} by a space-dependant phase that any standard intensity detector is insensitive to.

3. Non-isoplanatism of a thin lens

The scenario exhibited in the simple example of the pinhole camera actually occurs in all optical imaging systems. When imaging with lenses or mirrors, however, the diffraction effects are less dramatic than with a pinhole camera. The problem of phase distortion remains though, and may sometimes induce unwanted intensity modulation in the image.

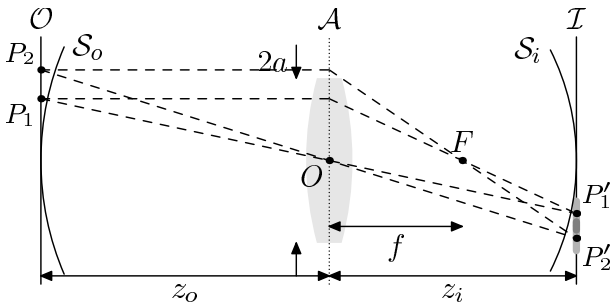


Fig. 3. Scheme of coherent image formation by an aberration-free thin lens. The points P'_1 and P'_2 in the image plane \mathcal{I} are the geometrical images of the point objects P_1 and P_2 in the object plane \mathcal{O} . The light-gray zones around P'_1 and P'_2 in the \mathcal{I} -plane represent the individual diffraction patterns resulting from illumination of the pinhole by P_1 and P_2 respectively. The dark-gray zone represents the area where the individual diffraction patterns overlap and interfere.

An aberration-free thin lens is an ideal diffraction-limited optical system that acts locally on the impinging field as a pure phase transparency $T(x, y) = \exp[-i\pi(x^2 + y^2)/(\lambda f)]$, where f is the focal length of the lens. The impulse response function of a thin lens [4,2] is an important concept that has proven to be very useful for the design of optical systems and optical data processing. It turns out that it is given by the same formula as for the pinhole camera — Eq. (3) — with the understanding that z_i is now related to z_o through the lens law $1/z_o + 1/z_i = 1/f$. To stress the analogy between the pinhole camera and the thin lens systems, we have drawn on Fig. 3 the same information as on Fig. 1, and used the same notation. In particular, note that $2a$ now represents the diameter of the lens, which is usually considerably larger than the aperture of the pinhole camera. As a consequence, the diffraction effects will be weaker, and non-isoplanatism will be less pronounced. Apart from this comment, the results and discussion of the last section also apply to the thin lens system. The relation between the field distribution in the plane \mathcal{O} and its image on the plane \mathcal{I} is non-isoplanatic and is given by Eq. (4). As with the pinhole camera, isoplanatism can be recovered — Eq. (5) — when the thin lens is used to image the spherical surface \mathcal{S}_o to \mathcal{S}_i . However, this is much less obvious here because, in contrast with the pinhole camera, a lens does not have an infinite field of view. That \mathcal{S}_i is the image sur-

face of \mathcal{S}_o is therefore questionable. This point requires a more careful argumentation that we postpone to Sec. 5.

Whether non-isoplanatism leads to interference when a plane emitter is imaged to a plane receptor depends not only on the size of the lens, but also on the size of the object and its position with respect to the optical axis. The condition for avoiding any interferences due to non-isoplanatism is that the phase $2\pi r/\lambda$ in Eq. (4) varies by less than π when the point corresponding to coordinates (x_o, y_o) explores the Airy pattern $\delta_{\frac{a}{\lambda z_o}}(x_i/M - x_o, y_i/M - y_o)$ in the object plane. If this is the case, the phase factor $\exp[i2\pi r/\lambda]$ can be taken out of the integral in Eq. (4). Since the fastest phase variation occurs when the point moves radially off axis, the following condition is obtained:

$$e_o \left(\rho_o^g + \frac{e_o}{4} \right) \ll \lambda z_o, \quad (6)$$

where $\rho_o^g = \sqrt{(x_i/M)^2 + (y_i/M)^2}$ is the off-axis distance of the geometrical object point under consideration and $e_o = 1.22\lambda z_o/a$ is the first-zero full width of the Airy pattern in the object plane. Note that Tichenor and Goodman [4] found a similar condition following a different reasoning. The main conclusions are:

- When imaging points very close to the optical axis ($\rho_o^g \ll e_o/4$), interference due to non-isoplanatism does not occur if $a^2/\lambda z_o \gg 1$. This last condition is always satisfied in practice with lenses. (For a diffraction-limited pinhole camera it fails to be satisfied.)
- When imaging off-axis points ($\rho_o^g \gg e_o/4$), interference due to non-isoplanatism does not occur if $\rho_o^g \ll a$, i.e. if the object points are not as far off-axis as the edges of the lens.

When criterion (6) is satisfied for any point on the object, Eq. (4) can be written as

$$U_i(x_i, y_i) = \frac{1}{|M|} e^{i\pi \frac{x_i^2 + y_i^2}{\lambda(z_i - f)}} \iint U_o(x_o, y_o) \delta_{\frac{a}{\lambda z_o}} \left(\frac{x_i}{M} - x_o, \frac{y_i}{M} - y_o \right) dx_o dy_o, \quad (7)$$

where the phase factor comes from the second order approximation of $s(x_i, y_i) + r(x_i/M, y_i/M)$ and constant phases have been removed. An intensity detector in the plane \mathcal{I} will record the same image as in the isoplanatic case — Eq. (5). It should however be noted that the impulse response function is still *non-isoplanatic* because the phase curvature has not been removed. It is important to keep this in mind when a phase-sensitive detector (hologram) is used and/or if further optical processing is needed.

4. Non-isoplanatism and large field imaging

According to the discussion in Sec. 3, non-isoplanatism has no effect on the intensity detected in the image plane if condition (6) is satisfied. In that case, Eq. (7) can be used instead of Eq. (4). In practical applications of coherent imaging, the assumption is usually made [2] that the field

mapping from the object space to the image space *is* given by Eq. (7) for any lens of a given optical system. This assumption is very convenient from a theoretical point of view since it makes the analysis of optical systems much simpler by the use of standard Fourier optics methods. From a technical point of view, however, good quality lenses (aspheric lenses, for instance) usually have a small diameter because of manufacturing constrains, and care must therefore be taken when implementing optical systems based on Eq. (7). In this section, we show that the slight difference between Eqs. (7) and (4) may lead to strong effects if the object does not fulfill condition (6).

Let's first point out what is wrong with Eq. (7) from a physical point of view. Consider an object field $U_o(x_o, y_o)$ that is varying slowly on the length scale $e_o = 1.22\lambda z_o/a$ of the peaked function $\delta_{a/(\lambda z_o)}(x_i/M - x_o, y_i/M - y_o)$. Then, according to Eq. (7), one can write

$$|U_i(x_i, y_i)|^2 = \frac{1}{|M|^2} \left| U_o \left(\frac{x_i}{M}, \frac{y_i}{M} \right) \right|^2. \quad (8)$$

This equation implies that the energy is conserved: $\iint |U_i(x_i, y_i)|^2 dx_i dy_i = \iint |U_o(x_o, y_o)|^2 dx_o dy_o$. However, independently of how slowly the field varies in space, Eq. (8) cannot hold for far off-axis points when the lens has a limited aperture. Radiation from far off-axis points (like P_2 on Fig. 3) is partially lost, and energy cannot be conserved. For instance, in the case of a plane wave travelling along the optical axis, radiation from the neighborhood of P_2 will not be transmitted at all. We can therefore conclude that Eq. (7) does not properly account for energy loss due to the limited aperture of the lens, especially for light originating from far off-axis points. Taking the phase factor $\exp(i2\pi r/\lambda)$ out of the integral sign in Eq. (4) breaks down the energy balance.

To give a deeper insight of the effect of the phase factor $\exp(i2\pi r/\lambda)$, we use Eq. (4) instead of Eq. (7) to compute the intensity distribution in the image plane for a slowly varying object field. We now obtain

$$|U_i(x_i, y_i)|^2 = \frac{1}{|M|^2} \left| U_o \left(\frac{x_i}{M}, \frac{y_i}{M} \right) \right|^2 \times \left| \iint e^{i\frac{2\pi}{\lambda z_o}(x_o^2 + y_o^2)} \delta_{\frac{a}{\lambda z_o}} \left(\frac{x_i}{M} - x_o, \frac{y_i}{M} - y_o \right) dx_o dy_o \right|^2$$

instead of Eq. (8). The paraxial approximation $r \approx z_o + (x_o^2 + y_o^2)/(2z_o)$ has been used. Making a change of integration variables from (x_o, y_o) to $(\xi, \eta) = (x_o, y_o) - (x_i, y_i)/M$, the preceding equation can be written as

$$|U_i(x_i, y_i)|^2 = \frac{1}{|M|^2} \left| U_o \left(\frac{x_i}{M}, \frac{y_i}{M} \right) \right|^2 \times \left| \iint e^{i\frac{2\pi}{\lambda z_o} \left(\frac{x_i}{M}\xi + \frac{y_i}{M}\eta + \frac{\xi^2}{2} + \frac{\eta^2}{2} \right)} \delta_{\frac{a}{\lambda z_o}}(\xi, \eta) d\xi d\eta \right|^2. \quad (9)$$

The integral in Eq. (9) has the form of a *Fresnel diffraction integral*. For points (x_i, y_i) which are sufficiently far away from the optical axis, the quadratic phase terms $\xi^2/2$ and $\eta^2/2$ can, as a first order approximation, be neglected, and

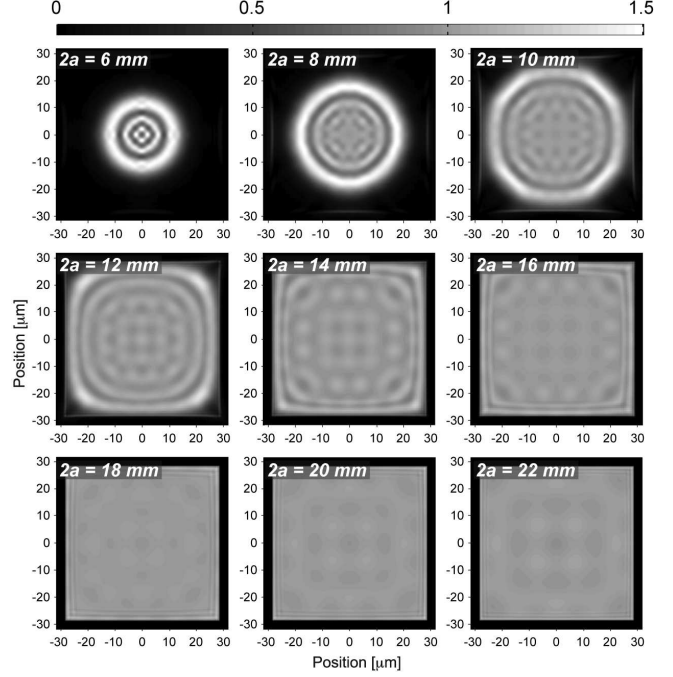


Fig. 4. Intensity in the image plane \mathcal{I} when a large square aperture, centered on the optical axis, is imaged with a thin lens. The square aperture is illuminated by a plane wave travelling along the optical axis. The sides of the square are $b = 9.5$ mm. The different panels correspond to different lens diameters. From left to right and top to bottom, the lens diameter is progressively increased in 2 mm-steps from $2a = 6$ mm to $2a = 22$ mm. The relevant parameters are: $\lambda = 780$ nm, $f = 12$ mm, and $z_o = 2$ m. The scale of the figures is expressed in microns. The intensity scale is such that 1 corresponds to the expected uniform intensity in the center of the square in the limit of an infinite lens.

the integral reduces to the Fourier transform of the Airy pattern in the object space. Using

$$\iint e^{i2\pi(x\xi + y\eta)} \delta_N(\xi, \eta) d\xi d\eta = \text{circ} \left(\frac{x}{N}, \frac{y}{N} \right), \quad (10)$$

Eq. (9) becomes

$$|U_i(x_i, y_i)|^2 = \frac{1}{|M|^2} \left| U_o \left(\frac{x_i}{M}, \frac{y_i}{M} \right) \right|^2 \times \text{circ}^2 \left(\frac{x_i}{Ma}, \frac{y_i}{Ma} \right). \quad (11)$$

In Eqs. (10) and (11),

$$\text{circ}(x, y) = \begin{cases} 1 & \text{if } \sqrt{x^2 + y^2} < 1, \\ 0 & \text{if } \sqrt{x^2 + y^2} > 1. \end{cases} \quad (12)$$

Eq. (11) shows that the intensity in the image plane exhibits a cut-off. No intensity reaches the image plane at a distance higher than Ma from the optical axis. This can be understood in the following way: since the field has been assumed to be slowly varying, the diffraction in the propagation from the object plane to the lens is negligible and the limited aperture of the lens has the same effect as a stop of radius a in the object plane. The function $\text{circ}(x_i/(Ma), y_i/(Ma))$ is the image of that virtual stop and can be interpreted as the shadow of the lens. This is, however, only a first order

approximation, since the quadratic phase terms $\xi^2/2$ and $\eta^2/2$ in Eq. (9) have been neglected. The effect of these quadratic phase terms is to create radial intensity oscillations in the image, especially around the cut-off radius Ma .

In Fig. 4, the preceding discussion is illustrated with an example. A square object of size $9.5 \times 9.5 \text{ mm}^2$ is imaged using a lens of diameter $2a$ varying from 6 mm to 22 mm. The object can be seen as a plane screen with a square aperture in it which is illuminated by a plane wave propagating along the optical axis. The object field $U_o(x_o, y_o)$ is 1 inside the square and zero outside of it. Fig. 4 shows the intensity distribution in the image plane computed using Eq. (4). With small lenses ($2a$ up to 10 mm) the clipping predicted by Eq. (11) is observed. One can clearly distinguish the disk (12) that limits the observable part of the object, as well as the intensity ripples due to the quadratic phase terms in (9) which were neglected when deriving (11). Interestingly, the intensity oscillations do not disappear as soon as the lens becomes bigger than the object. For $2a = 22 \text{ mm}$, some residual modulation still remains. Note that the parameters of this simulation are realistic ones: the object distance z_o has been fixed to 2 m (close to infinite-conjugate ratio imaging) and the focal length f to 12 mm (the numerical aperture ranges from 0.24 to 0.67). Note that energy is lost when imaging large objects through small lenses: For the simulations shown in Fig. 4, the percentage of transmitted energy is, from left to right and top to bottom, 31.1%, 56.1%, 83.4%, 96.6%, 99.2%, 99.8%, and nearly 100% for the last three images.

The discussion leading to Eqs. (8) to (11) only concerned object fields $U_o(x_o, y_o)$ that are slowly varying on the length scale $e_o = 1.22 \lambda z_o/a$ in the object plane. For quickly varying fields the previous discussion does not hold, but non-isoplanatism still has some effects on imaging. The way non-isoplanatism modifies the intensity distribution in the image plane strongly depends on the object wavefront. No general features can be drawn in that case. To get some insight, consider the following example.

A large square grid ($19 \times 19 \text{ mm}^2$) of mutually coherent point sources is imaged through a lens of diameter $2a = 8 \text{ mm}$. The imaging conditions are otherwise the same as in Fig. 4. Let's consider that all the point sources are in phase and discuss the image formation when the spacing d between the point sources is varied. If the points are well separated ($d \gg e_o/2$, so that the Airy patterns associated with them in the image plane do not overlap) no interference takes place and non-isoplanatism has no effect on the intensity distribution in the image plane. If the Airy patterns overlap, interferences similar to those depicted in Fig. 2 occur. Two cases must be distinguished: $d \ll e_o/2$ and $d \approx e_o/2$. For $d \ll e_o/2$, the object field varies slowly in space; a fringe pattern similar to the one in Fig. 4 is expected. The interesting case is $d \approx e_o/2$. Fig. 5 shows the intensity distribution in the image plane when d ranges from 0.6 to 2.2 times $e_o/2$. For $d \leq e_o/2$, a fringe pattern similar to the one in Fig. 4 is seen in the center of the field. However, periodic replicas of this pattern are also observed. For $d >$

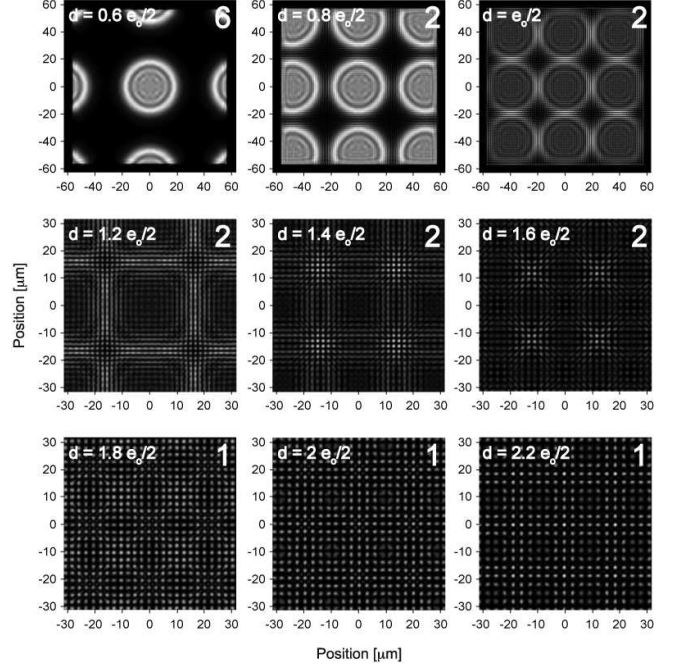


Fig. 5. Intensity in the image plane \mathcal{I} when a large squared ($19 \times 19 \text{ mm}^2$) grid of point sources, centered on the optical axis, is imaged by a thin lens. The point sources are mutually coherent and in phase. The different panels correspond to different values of the grid period d . From left to right and top to bottom, d is varied from $0.6 e_o/2$ to $2.2 e_o/2$ ($e_o/2$ is the separation corresponding to the Rayleigh resolution criterion). The relevant parameters are: $a = 4 \text{ mm}$, $\lambda = 780 \text{ nm}$, $f = 12 \text{ mm}$, and $z_o = 2 \text{ m}$. The scale of the figures is expressed in microns. The intensity scale is arbitrary but the relative dynamical range is indicated by the number in the upper right corner of each panel. For instance, the number “6” in the first panel means that the intensity range is 6 times larger than in the three panels of the last row.

$e_o/2$, the circular fringe patterns intersect each other, but the sparse sampling due to the grid structure of the image makes this structure barely visible (periodicity however remains). For clarity, only the central $30 \times 30 \mu\text{m}^2$ region of the image is displayed in the last six panels of Fig. 5. The simulations of Fig. 5 show that the intensity distribution in the image plane exhibit two distinct pseudo-periods (in both x and y directions): the small-scale pseudo-period Md due to the grid structure of the object and the large-scale pseudo-period X associated with the ring patterns due to non-isoplanatism. Strictly speaking the image is periodic only if X is an integer multiple of Md , in which case the period of the image is X . Hereafter, we use this property to deduce the value of X . The object field is modelled as a two-dimensional Dirac comb:

$$U_o(x_o, y_o) = \sum_{n,m} \delta(x_o - n d, y_o - m d),$$

where the integers n and m run from $-\infty$ to $+\infty$. Using Eq. (4), we then find that

$$|U_i(x_i, y_i)|^2 = \frac{1}{|M|^2} \times$$

$$\left| \sum_{n,m} e^{i\phi_{nm}} \delta_{\frac{a}{\lambda z_o}} \left(\frac{x_i}{M} - nd, \frac{y_i}{M} - md \right) \right|^2, \quad (13)$$

with

$$\phi_{nm} = \frac{\pi}{\lambda z_o} (n^2 + m^2) d^2.$$

In order to find X , we require that $|U_i(x_i, y_i)|^2 = |U_i(x_i + X, y_i)|^2$ when X is a multiple of Md . Using eq. (13), we have

$$|U_i(x_i + X, y_i)|^2 = \frac{1}{|M|^2} \times \left| \sum_{n,m} e^{i\phi_{nm}} \delta_{\frac{a}{\lambda z_o}} \left(\frac{x_i + X}{M} - nd, \frac{y_i}{M} - md \right) \right|^2.$$

The argument $(x_i + X)/M - nd$, can be rewritten as $x_i/M - n'd$ with $n' = n - X/(Md) \in \mathbb{Z}$. Replacing the sum over n by a sum over the values of n' , we obtain

$$|U_i(x_i + X, y_i)|^2 = \frac{1}{|M|^2} \times \left| \sum_{n',m} e^{i\phi_{n'm}} \delta_{\frac{a}{\lambda z_o}} \left(\frac{x_i}{M} - n'd, \frac{y_i}{M} - md \right) \right|^2.$$

where

$$\phi_{n'm} = \frac{\pi}{\lambda z_o} \left[n'^2 + 2n' \frac{X}{Md} + m^2 \right] d^2.$$

One can note that $\phi_{n'm}$ and ϕ_{nm} just differ by a factor $n' \times 2\pi$, and therefore $|U_i(x_i, y_i)|^2 = |U_i(x_i + X, y_i)|^2$, if X is given by

$$X = M \times \frac{z_o \lambda}{d}. \quad (14)$$

When X is not a multiple of Md , formula (14) is still valid if X is understood as the large-scale pseudo-period. However, the notion of ‘‘large-scale pseudo-period’’ only holds if $X/(Md) \approx a e_o/d^2 \gg 1$ ($e_o = 1.22 \lambda z_o/a$). Since a/d is usually a large number, this condition can still be valid even if d strongly exceeds the distance $e_o/2$ corresponding to the Rayleigh criterion. The periodic patterns displayed in Fig. 5 prove that the field in the image plane corresponding to the Airy pattern of a given point in the grid influences the entire image on a length scale much longer than the usually considered ‘‘Airy pattern diameter’’ e_o . Readers familiar with signal processing will notice that the reason why periodicity appears here is the same one that makes the Fourier spectrum of a sampled signal (Dirac comb) periodic. We however stress that the periodicity that is described here appears in the image plane *and not* in the Fourier plane of the object field. This is a peculiarity of non-isoplanatic imaging.

Though non-isoplanatism can strongly influence the image formation of both slowly varying and rapidly varying object fields, the effects are qualitatively different. For slowly varying fields, we have seen that the major effect

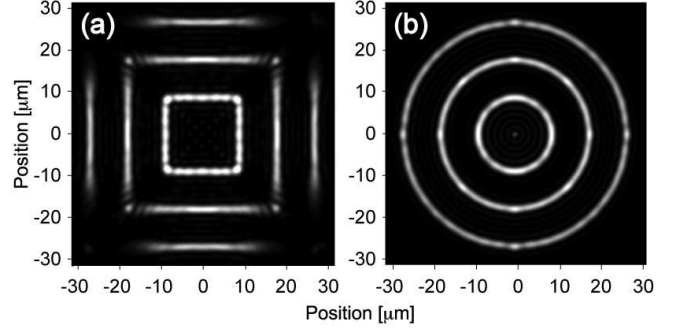


Fig. 6. Intensity in the image plane \mathcal{I} when squared and circular contours are imaged by a thin lens. In the object plane, all the point sources forming the contours are mutually coherent and in phase. The imaging conditions are the same as in Fig. 4 ($\lambda = 780$ nm, $f = 12$ mm, and $z_o = 2$ m), but the size of the lens is fixed: $2a = 6$ mm, as in the first panel of Fig. 4. The intensity scale is arbitrary. Panel (a) shows the image of three squared contours of increasing side $b = a$, $b = 2a$ and $b = 9.5$ mm $\approx 3.2 a$. The size of the outer square is the same as in Fig. 4. Panel (b) shows the image of three concentric circles, the diameters of which are equal to the sides of the squares in the panel (a).

comes from the shadow that the lens projects in the image plane. The image is clipped so that only the central disk of radius Ma remains (see Fig. 4). The simulations of Fig. 5 show that, for rapidly varying object fields, light *is* observed outside the central disk of radius Ma . More complex effects are exhibited, but clipping do not occur anymore. In many applications of coherent optics (like optical lithography), the object is made of lines instead of single points or filled surfaces. Lines are objects on which the field varies slowly in one direction (the direction tangent to the line) and rapidly in the orthogonal one. Therefore, one can expect that the effects of non-isoplanatism will be intermediate between the two previous cases. Fig. 6 helps to understand how lines are imaged through a non-isoplanatic optical system. The imaging conditions are the same as in Fig. 4, except that the lens diameter is fixed: $2a = 6$ mm. Panel (a) shows the image of three squared contours. The outer square is exactly the contour of the filled square imaged in Fig. 4. The comparison with the upper-left panel of Fig. 4 shows that the major part of the contour is now visible; only the corners of the square are clipped. Closer examination shows that, for a straight line, only a segment of length $2a$ in the object plane ($2Ma$ in the image plane) is transmitted. The part of the line that is clipped corresponds to the orthogonal projection of the shadow of the lens on the straight line. This can be easily understood by analysing the propagation of the cylindrical waves emitted by straight lines through the spherical lens. The smaller square in panel (a) is transmitted because its side is shorter than the diameter of the lens. The intermediate square is at the limit of the cut-off. As shown in the panel (b) of Fig. 6, circles are never clipped, whatever their radii, because the orthogonal projection of the lens disk on the circle is the circle itself.

5. Isoplanatic imaging through a thin lens

In Sec. 3, we claimed that isoplanatic imaging is possible with a thin lens when the object lies on the spherical surface \mathcal{S}_o and the image is observed on the spherical surface \mathcal{S}_i . Let's examine this statement more closely.

Referring to Fig. 3, simple Gaussian Optics arguments suggest that if the point P_2 is translated horizontally from the object plane \mathcal{O} to the surface \mathcal{S}_o , its image P'_2 , instead of moving towards \mathcal{S}_i , should move away from the lens. This argument is correct, but it relies on the Gaussian approximation that the point P'_2 is initially in the “image plane” \mathcal{I} . In reality, because of the field curvature aberration due to the lens, the stigmatic image of P_2 is closer to the lens than the surface \mathcal{S}_i itself (P'_2 lies on the so-called Petzval surface). Bringing P_2 on \mathcal{S}_o will place its image P'_2 exactly on \mathcal{S}_i [11]. Consequently, Eq. (5) is exact, while Eq. (4) is only valid in the context of Gaussian approximation. If the lens is still diffraction-limited in this regime (no point-aberrations), the isoplanatic imaging geometry provides a nearly perfect transfer of the coherent field from the object to the image space. Only the resolution is reduced because of the finite size of the lens.

The problem that remains is how to transfer a given field from a plane surface to a curved one before imaging, and vice versa after imaging. Generally, the object field is obtained by modulating a coherent illumination field $A(x_o, y_o)$ by a complex amplitude function $u_o(x_o, y_o)$:

$$U_o(x_o, y_o) = A(x_o, y_o) \times u_o(x_o, y_o). \quad (15)$$

The modulation $u_o(x_o, y_o)$ can be produced by any plane modulation device like a plane transparency, a grating or some kind of adaptative optics. Usually $u_o(x_o, y_o)$ itself is considered as the “object” of interest. In that case, the illumination beam must be a plane wave propagating along the optical axis in order to map the profile $u_o(x_o, y_o)$ to the beam: $U_o(x_o, y_o) \propto u_o(x_o, y_o)$. If, instead, we illuminate the modulation device with a spherical wave $A(x_o, y_o) = A \exp(-i2\pi r/\lambda)$ focusing on \mathcal{O} (see Fig. 3), we get $U_{\mathcal{S}_o}(x_o, y_o) = U_o(x_o, y_o) \exp(i2\pi r/\lambda) \propto u_o(x_o, y_o)$. This kind of illumination projects the object onto \mathcal{S}_o as required for isoplanatic imaging [2]. Starting with an illuminating plane wave travelling along the optical axis, this can be achieved by placing an additional thin lens of focal length z_o just before (or just after) the object plane \mathcal{O} . This lens must act as a pure phase-correction transparency. Similarly, on the image side, a thin lens of focal length z_i placed just after (or before) the image plane can be used to project the image from \mathcal{S}_i onto \mathcal{I} . From a broader point of view, any spherical field distribution in the object space of a centered paraxial optical system can be imaged onto a spherical surface of any curvature using only lenses; some of them will be imaging lenses, while others will play the role of phase-correction transparencies. This is the basis of the so-called *metaxial optics* theory formulated by the Bonnet [12–14].

It should be noted that this approach only works for sufficiently slowly varying fields, because the diffraction from \mathcal{O} to \mathcal{S}_o (and \mathcal{S}_i to \mathcal{I}) has to be negligible for the amplitude of the fields on \mathcal{O} and \mathcal{S}_o (\mathcal{S}_i and \mathcal{I}) being the same. In addition, due to optical design constraints, the use of optical lenses as phase-correction transparencies is not always possible. Moreover, lenses are never perfectly thin and diffraction through them may have worse effects on imaging than the phase curvature due to non-isoplanatism. Whether or not non-isoplanatism should be corrected depends on the particular system under consideration. A clever design can minimize, if not cancel, its effects on the detected intensity.

6. Experimental investigation

The theoretical discussion of Secs. 4 and 5 relies on two strong approximations: the paraxial approximation and the thin lens approximation. One may wonder whether our analysis is robust enough to be applied to systems containing powerful lenses, which are usually thick and have a high numerical aperture. The following experiment shows that the previous discussion is also valid for these systems.

The setup is shown in Fig. 7. The test lens L_1 is an aspheric lens having a focal length $f = 8$ mm and a diameter $2a = 8$ mm (LightPath 352240). This lens is used to image the surface of a spatial light modulator (SLM), a 1024×768 micromirror array, that modulates the amplitude of the reflected beam. Using the SLM, we can generate arbitrary patterns. The resolution is set by the size of the micromirrors ($13 \times 13 \mu\text{m}^2$). The object plane is 60 cm away from the lens. We use a double-lens system (L_3, L_4) to magnify the image produced and project it on the CCD camera. L_3 is a diffraction-limited aspheric lens and L_4 a long-focal achromatic doublet. The numerical aperture of this double-lens system is large enough to prevent any possible clipping or diffraction during the magnification process. The SLM is either illuminated with a plane wave or a spherical wave converging on L_1 ($\lambda = 780$ nm). In the first case, the imaging system is non-isoplanatic. As explained in Sec. 5, it becomes isoplanatic when a spherical-wave illumination is used. The spherical wave is obtained from the impinging plane wave by inserting the additional lens L_2 (75-cm focal length, achromatic doublet) in front of the SLM. We use this setup to image objects of different sizes and shapes through the test lens.

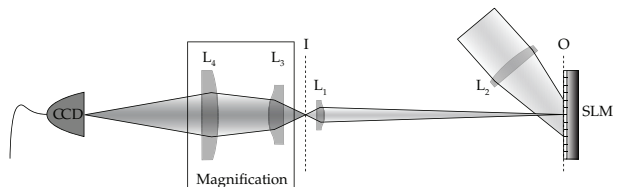


Fig. 7. Experimental setup: L_1 , aspheric lens ($f = 8$ mm); L_2 , achromatic doublet ($f = 750$ mm); L_3 , aspheric lens ($f = 20$ mm); and L_4 , achromatic doublet ($f = 500$ mm); SLM, spatial light modulator; CCD, coupled-charge camera; O, object plane; I, image plane.

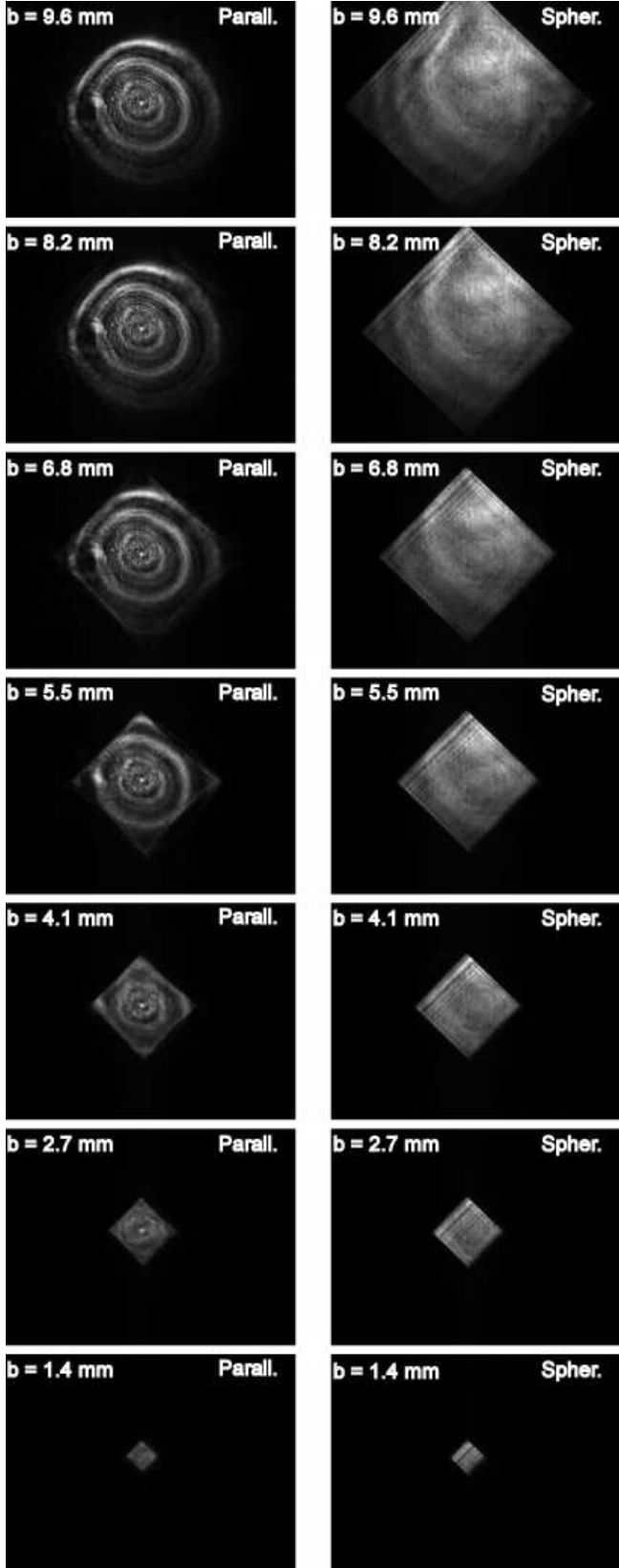


Fig. 8. Images of different-sized squares (the side b ranges from 1.4 mm to 9.6 mm) recorded using the setup in Fig. 7. The object plane is either illuminated with a parallel beam (non-isoplanatic case, left column) or with a spherical one converging on L_1 (isoplanatic case, right column).

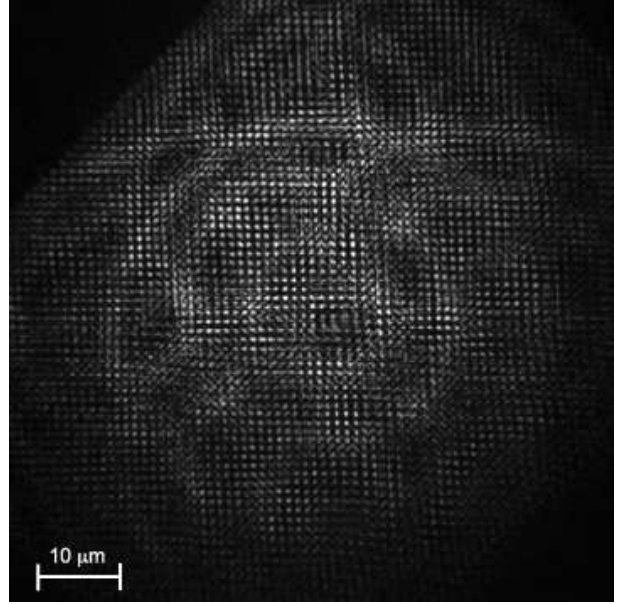


Fig. 9. Images of a rectangular grid of points recorded using the setup in Fig. 7. The object plane is illuminated with a parallel beam (non-isoplanatic case). The period of the grid in the object plane, $d = 109 \mu\text{m}$, corresponds to 1.5 times the Rayleigh criterion separation ($e_o/2$).

Fig. 8 shows the pictures recorded by the CCD camera when we image squares of different sizes through the 8-mm diameter aspheric lens L_1 . Let's first consider the case when the SLM is illuminated by a parallel beam (non-isoplanatic imaging, left column of Fig. 8). For a square side larger than 8 mm, the clipping effect described in Sec. 4 is clearly observed. Circular fringes similar to those of Fig. 4 are also seen in the image plane. For a square side smaller than 8 mm, the region of non-zero intensity is limited by the size of the square. However, intensity modulation due to non-isoplanatism is still noticeable for a square side as small as 2.7 mm. In the case of the $1.4 \times 1.4 \text{ mm}^2$ square, non-isoplanatism has a negligible effect. Note that, in the simulations of Fig. 4, the lens size was varied while the object size was kept constant. Here, the lens is always the same, but the square size is varied instead. For this reason, the ring pattern is the same for every picture in the left column of Fig. 8. When the SLM is illuminated with a spherical wave converging on L_1 (isoplanatic imaging, right column of Fig. 8) no clipping effect occurs and there is, in principle, no limit to the size of the objects that the system can image (the slight variations in intensity are due to amplitude inhomogeneities in the illumination beam).

In a second experiment, we imaged rectangular grids of points illuminated by a plane wave (non-isoplanatic illumination), a situation that we described theoretically in Sec. 4. Fig. 9 shows the recorded intensity distribution in the image plane for a grid with a period $d = 109 \mu\text{m}$, which corresponds to 1.5 times the Rayleigh criterion separation ($e_o/2$). As shown in Sec. 4, for such large value of d the ring patterns should not be visible anymore (see the six last panels of Fig. 5). Here, however, we can distinguish one

central ring pattern and four replicas intersecting it. We attribute this discrepancy to the fact that the experimental point-spread function is a bit broader than the theoretical Airy pattern. As noted in Sec. 4, the “disappearance” of the multiple ring patterns when d increases is caused by the sparseness of sampling due to the grid. A broadening of the point-spread function reduces that sparseness and therefore restores the ring patterns characteristic of non-isoplanatic imaging.

7. Conclusion

In general, even diffraction-limited imaging systems distort the phase of the processed fields. This is of no relevance when used with incoherent light, but has a tremendous effect on coherent imaging. In combination with Fraunhofer diffraction from the finite instrumental aperture, the phase distortion leads to a severe degradation of the field amplitude in the image plane. We analyzed this phenomenon for two very different but prototypic imaging systems (the pin-hole camera and a thin lens) and observed its fundamental and general nature. We showed that substantially different effects arise depending on whether the field varies slowly or rapidly on the length scale of an Airy pattern. The degradation of the field amplitude can however be overcome or, at least, limited by a clever design of the optical system. The main aspects of our analysis have been confirmed experimentally using a powerful thick aspheric lens to demonstrate that the phenomenology that is described also holds beyond the paraxial and thin lens approximations used for the theoretical analysis.

Acknowledgments

We gratefully acknowledge support by the Engineering and Physical Sciences Research Council (EP/E023568/1), the QIP IRC (GR/S82176/01), the Research Unit 635 of the German Research Foundation, and the EU through the research and training network EMALI (MRTN-CT-2006-035369) and the integrated project SCALA. One of us (E. B.) also wishes to express his gratitude to the Philippe Wiener and Maurice Anspach Foundation.

References

- [1] M. Born and E. Wolf, *Principles of Optics* Seventh Ed., Cambridge University Press, Cambridge, 2006
- [2] J. W. Goodman, *Introduction to Fourier Optics* Third Ed., Roberts & Company, Englewood, 2005
- [3] P. Dumontet, *Optica Acta* 2 (1955) 53-63
- [4] D. A. Tichenor and J. W. Goodman, *J. Opt. Soc. Am.* 62 (1972) 293-295
- [5] T. Ito and S. Okazaki, *Nature* 6799 (2000) 1027-1031
- [6] J. F. Heanue, M. C. Bashaw, L. Hesselink, *Science* 265 (1994) 749-752
- [7] L. Brandt, C. Muldoon, E. Brainis, and A. Kuhn, in: *CLEO/QELS-Phast 2008 Technical Digest*, OSA, Washington DC, JThA1005.
- [8] D. Meschede and A. Rauschenbeutel, in: G. Rempe and M. O. Scully (Eds.), *Adv. At. Mol. Opt. Phys.*, vol. 53, Academic Press, London, 75-104, 2006
- [9] Y. Miroshnychenko, W. Alt, I. Dotsenko, L. Förster, M. Khudaverdyan, D. Meschede, D. Schrader, and A. Rauschenbeutel, *Nature* 442 (2006) 151-151
- [10] S. Bergamini, B. Darquié, M. Jones, L. Jacubowicz, A. Browaeys, and P. Grangier, *JOSA B* 21 (2004) 1889-1894
- [11] E. Hecht, *Optics* Fourth Ed., Addison Wesley, San Francisco, 2002
- [12] G. Bonnet, *Ann. Télécommunic.* 33 (1978) 143-165
- [13] G. Bonnet, *Ann. Télécommunic.* 33 (1978) 225-243
- [14] G. Bonnet, in: *Septième colloque sur le traitement du signal et ses applications*, 54/1-8, GRETSI-Actes de Colloques (<http://hdl.handle.net/2042/10360>), 1979